International Journal of Nanomedicine

Dovepress
open access to scientific and medical research

Open Access Full Text Article

ORIGINAL RESEARCH

Modified methods of nanoparticles synthesis in pH-sensitive nano-carriers production for doxorubicin delivery on MCF-7 breast cancer cell line

This article was published in the following Dove Press journal:
International Journal of Nanomedicine

Ahmed Hamidu[1,2]
Ajat Mokrish[3]
Rozaihan Mansor[3]
Intan Shameha Abdul Razak[3]
Abubakar Danmaigoro[3]
Alhaji Zubair Jaji[3]
Zuki Abu Bakar[1]

[1]Laboratory of Molecular Biomedicine, Institute of Bioscience, Universiti Putra Malaysia, Serdang 43400, Selangor, Malaysia; [2]Department of Sciences and Engineering, Federal Polytechnic Mubi, Adamawa State, Nigeria; [3]Department of Preclinical Science, Faculty of Veterinary Medicine, Universiti Putra Malaysia, Selangor 434000, Selangor, Malaysia

Purpose: Modified top-down procedure was successfully employed in the synthesis of aragonite nanoparticles (NPs) from cheaply available natural seawater cockle shells. This was with the aim of developing a pH-sensitive nano-carrier for effective delivery of doxorubicin (DOX) on MCF-7 breast cancer cell line.

Methods: The shells were cleaned with banana pelts, ground using a mortar and pestle, and stirred vigorously on a rotary pulverizing blending machine in dodecyl dimethyl betane solution. This simple procedure avoids the use of stringent temperatures and unsafe chemicals associated with NP production. The synthesized NPs were loaded with DOX to form DOX-NPs. The free and DOX-loaded NPs were characterized for physicochemical properties using field emission scanning electron microscopy, transmission electron microscopy, zeta potential analysis, Fourier transform infrared spectroscopy, and X-ray diffraction. The release profile, cytotoxicity, and cell uptake were evaluated.

Results: NPs had an average diameter of 35.50 nm, 19.3% loading content, 97% encapsulation efficiency, and a surface potential and intensity of 19.1±3.9 mV and 100%, respectively. A slow and sustained pH-specific controlled discharge profile of DOX from DOX-NPs was observed, clearly showing apoptosis/necrosis induced by DOX-NPs through endocytosis. The DOX-NPs had IC_{50} values 1.829, 0.902, and 1.0377 µg/mL at 24, 48, and 72 hrs, while those of DOX alone were 0.475, 0.2483, and 0.0723 µg/mL, respectively. However, even at higher concentration, no apparent toxicity was observed with the NPs, revealing their compatibility with MCF-7 cells with a viability of 92%.

Conclusions: The modified method of NPs synthesis suggests the tremendous potential of the NPs as pH-sensitive nano-carriers in cancer management because of their pH targeting ability toward cancerous cells.

Keywords: apoptosis, biomedical application, $CaCO_3$, nanoparticles and ultrastructure

Introduction

Nanomaterials have a wide range of applications in biomedical sciences, such as in therapeutic agents, diagnostic imaging systems, and drug delivery systems.[1,2] Cockle-shell-derived aragonite nanoparticles (NPs) have been reported as excellent and promising materials for therapeutics and antibiotic-loaded implants.[3,4] It was reported that calcium carbonate ($CaCO_3$) NPs have great potential efficient drug delivery systems. With biocompatibility and pH-sensitive properties[5] the anticancer drug doxorubicin (DOX) suggests its promising effects as a therapeutic agent in the clinical treatment of

Correspondence: Zuki Abu Bakar
Laboratory of Molecular Biomedicine, Institute of Bioscience, Universiti Putra Malaysia, Serdang, Selangor 43400, Malaysia
Tel +60 19 604 6659
Email zuki@upm.edu.my

tumors.[6,7] It has been shown in an earlier study that $CaCO_3$-DOX NPs have higher toxic effects on cancer cells compared to DOX alone.[8] The DOX/nanocrystals approach is vital for the enhancement of cancer therapy owing to the biodegradability, safety, and pH sensitivity of the system.[9] Furthermore, biobased aragonite $CaCO_3$-NPs have received vast attention amongst numerous researchers as a potential drug release agent.[5,10,11] In the recent utilization of $CaCO_3$-based NPs, spherical NPs have been designed as a novel delivery carrier for drugs and bioactive proteins, demonstrating sustained release in addition to high stability.[5,12] The present study focuses on the synthesis of cockle-shell-derived $CaCO_3$-NPs loaded with DOX as, a nano-anticancer carrier. The drug-loading capacity, encapsulation efficiency, and in vitro release profile of DOX-loaded $CaCO_3$-NPs were evaluated. The synthesized $CaCO_3$-NPs loaded with DOX were additionally evaluated for therapeutic efficacy against human breast cancer cells in vitro. $CaCO_3$ NPs with specific shape and sizes are very useful in biomedical applications.[13] These NPs have been reported as carriers with capabilities of retaining encapsulated drugs and bioactive proteins for sustained release at targeted cancer cells.[14] As a result, there is an increasing demand for the assembly of NPs with different morphologies, shapes, and sizes for various specialized areas.[15] Different methods of preparing $CaCO_3$-NPs have thus been reported for the delivery of soluble and insoluble drugs and bioactive proteins.[16] The increasing need for these nanocrystals for drug delivery should be met with improved techniques that enhance homogeneity to an optimal grade.[10,17] In this regard, the present study developed a simple, environmentally friendly method of cleaning cockle shells with banana pelt agent, followed by mechanical grinding and simple precipitation. This reproducible procedure enabled the synthesis of highly homogenized spherical nanocrystals.

Materials and methods

Materials

Cockle shells were purchased from a local Malaysian market. Dodecyl dimethyl betaine (BS-12) was purchased from Sigma-Aldrich (USA). Doxorubicin hydrochloride (DOX) was obtained from EMD Millipore Corporation (USA). PBS was acquired from (Sigma Aldrich St. Louis, MO, USA). All supplementary reagents were of analytical grade and used without modification unless stated otherwise in the experiment.

Preparation of micro-sized $CaCO_3$ powder from cockle shells

Cockle shells (*Anadara granosa*) were washed with tap water. The shells were then boiled for 30 min in a steel container and oven-dried (Member UM 5000, Germany) at 60°C. The dried shells were further washed in 100 mL of water containing squeezed banana pelt agent (Figure 1) at a ratio of 2:1 to remove stains and remaining debris on the cockle shells. The cockle shells were ground into powder form using a rotary pulverizing blending machine (RT-08 rpm 2500) and sieved at a pore aperture of 75 µm. The prepared cockle shell–based $CaCO_3$ powder was stored in a drying oven at 50°C before further analysis.

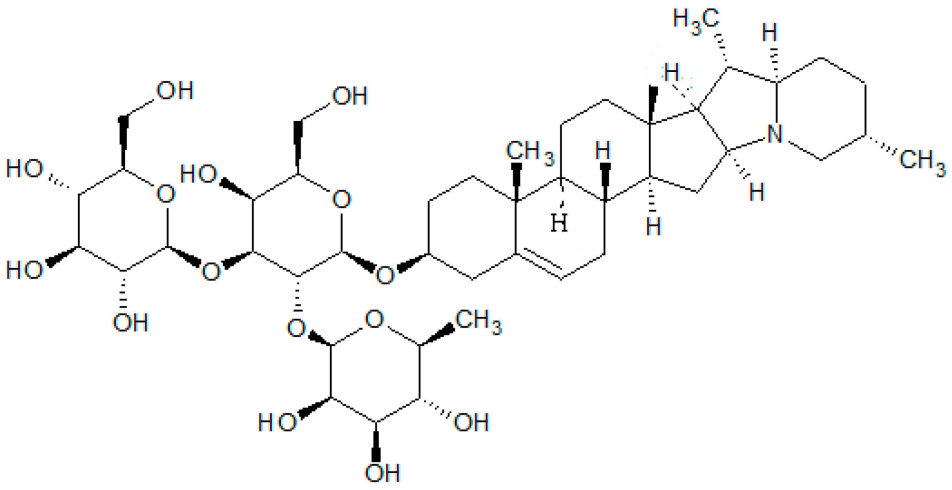

Figure 1 Molecular structure of banana peel.

Synthesis of nano-sized $CaCO_3$ from cockle shell-aragonite powder

Approximately 2 g of $CaCO_3$ powder with a size of 75 µm was added to 50 mL of deionized water. Then, 0.5 mL of BS-12 was added to the aqueous solution in a flat-bottom flask, and the solution was stirred at 1,000 rpm at 27°C for 2 hrs. After cooling, the aqueous solution was filtered with filter paper using deionized water and sediment NPs were allowed to dry in an oven for three days at 50°C.

Preparation of DOX-loaded $CaCO_3$-NPs (DOX-NPs)

One milligram of the DOX was added to 15 mg of $CaCO_3$ NPs suspension. The suspension was persistently stirred overnight in a dark room at 25°C. $CaCO_3$NPs containing DOX were centrifuged (Eppendorf, Centrifuge 5702 R, Germany) at 120 rpm, washed, and oven-dried at 25°C.

The following parameters were calculated;

$$\text{Loading content} = \text{Wt} - \text{Wf}/\text{Wnp} \times 100 \quad (1)$$

$$\text{Encapsulation efficiency} = \text{Wt} - \text{Wf}/\text{Wt} \times 100 \quad (2)$$

The mathematical equations were adapted from a previous report.[17]

Characterization of $CaCO_3$-NPs and DOX- NPs

Morphology and surface charge of $CaCO_3$-NPs and DOX-NPs

The physicochemical properties of the NPs were then analyzed by high-resolution transmission electron microscopy (HRTEM: H-7100 Hitachi, Tokyo, Japan) at a voltage of 5 kV and field-emission scanning electron microscopy (FESEM, JOEL JSM-7600F, USA) at 200 kV and 30 mA. The $CaCO_3$ NPs and DOX-NPs were dissolved in 90% ethanol and sonicated for 30 mins. From each suspension, one drop was loaded on top of a carbon-coated copper grid and dried at room temperature prior to viewing with TEM.[18] For FESEM, the samples were separately equipped on aluminum and coated with gold under an argon atmosphere by means of sputter coating measure using a Malvern Zeta-sized Nano ZS (Ver. 6.12, Serial no: MAL 1,042,820, Malvern Instruments). This measures the electrophoretic mobility of particles in an electrical field and then converts it into zeta potential.

Fourier-transform infrared spectroscopy (FT-IR)

FT-IR spectroscopy (Model 100 series, Perkin Elmer) was used to analyze the chemical properties of the $CaCO_3$ NPs, NPs, DOX-NPs, and free DOX and the absorption spectra of $CaCO_3$ 280–4000 cm^{-1} at a motion of 2 cm^{-1} and speed of 64 scan per second.

X-ray powder diffraction (XRD)

The purity and crystalline properties of NPs alone, DOX-NPs, and free DOX powders were examined using a Rigaku XRD. Traverse sections of the specimen were placed on a quartz plate for exposure to Cu Kα radiation wavelength of λ=1.5406 Ã. The samples were scanned at diffraction angles from 2° to 80° to obtain unique patterns of reflection peaks, at different angles and intensities at room temperature, over 2Θ ranges of 4–50°, and at sampling intervals 2θ=0.02° at a scanning rate of 0.6°/min.

In vitro drug release study

To evaluate the mechanism of synthesized NPs, the release profiles of DOX-NPs were examined in PBS solutions at pH 7.4 and 4 DOX-NPs were detached inside the aqueous buffer solution (1 mg/mL) and transferred to a dialysis membrane bag (molecular weight cutoff =10 kDa). The release experiment was initiated by placing the dialysis bag in 10 mL of discharge media. The media were shaking in (TU-400) at 37°C 100 rpm. At predetermined time intervals (0, 0.5, 2, 3, 6, 12, 24, 48, and 72 hrs), the samples were evaluated using ultraviolet visible spectrophotometry to quantify the concentration of DOX release.

Cell culture

The human breast cancer cell line (MCF-7) was selected for this study. MCF-7 was purchased commercially from the American Type Culture Collection (ATCC, Manassas, VA, USA). The cell line was cultured in high-glucose Dulbecco's modified Eagle medium containing 10% fetal bovine serum and 100 µg/mL penicillin and streptomycin at 37°C in 5% CO_2 incubator (Thermo Fisher Scientific, USA).

Cell line viability assay

The cells were seeded in 96-well plates (MCF-7 at 1×10^4 cells/well) and incubated for 24 hrs. To evaluate the biocompatibility of free NPs, MCF-7 cells were co-cultured with different concentrations of NPs for 24 hrs. For the cytotoxicity assay of DOX-NPs, MCF-7 cells were treated with different concentrations of DOX and DOX-NPs, for 24, 48, and 72 hrs. The NPs were sterilized with UV irradiation for 30 mins before use. Untreated cells served as the controls and nine wells without cells were used as blank controls. Subsequent

to the exposure, the cells were washed with PBS, and MTT reagent (5 mg/mL) was added and incubated at 37ºC for 4 hrs. The culture medium was discarded, and 200 µL of freshly prepared dimethyl sulfoxide was added to dissolve the formazan dye crystals into purple color. The absorbance was measured at 570 nm using a spectrophotometer microplate reader. Each assay was performed in triplicates. An IC_{50} standard, which signifies the drug concentration that inhibits 50% of the tested cells, acts as an indication of cell viability and was computed using the following equation:

$$\text{Cell viability}(\%) = \text{A test}/\text{A control} \times 100$$

where A test is the optical density of cells incubated with different treatments along and A control is the optical density of cells incubated with culture media only (negative control). The cytotoxicity was calculated from an average of three replicate tests and the results are expressed as mean ± standard deviation.

Apoptosis evaluation

Apoptosis of cells treated with DOX and DOX-NPs was evaluated by measuring the intrinsic fluorescence of DOX. MCF-7 cells were seeded in 6-well plates at a density of 5×10^5 cells/well. After 48 hrs of incubation, the medium was discarded and replaced with fresh medium, containing DOX or DOX-NPs with a corresponding DOX concentration of 0.5 µg/mL for 48 and 72 hrs at 37°C Acridine orange and propidium iodide were added into the culture medium to label control, apoptotic, and necrotic cells and then 1 mL of cells in the medium was transfer to a 15-mL tube after trypsinization. The cells were fixed, re-suspended in cold PBS, washed, and mounted on microscope slides. Fluorescence was visualized on fluorescence using a microscope (Nikon ELIPSE Ti S, Japan).

Ultrastructural microscopy of treated MCF-7 cells

The $IC_{50\ values}$ of DOX and DOX-NPs were used to induce apoptosis in MCF-7 cells. The cells were co-cultured with the NPs for 48 hrs. They were then trypsinized, centrifuged for 10 mins at 2000 rpm, and fixed in 4% glutaraldehyde for 24 hrs at 4ºC. The immobile cells were rinsed three times with of sodium coccadylate buffer for 10 mins each and post-fixed with 1% osmium tetroxide at 4°C for 2 hrs. Thereafter, the cells were dehydrated using acetone (35%, 50%, 75%, and 100%) and critical point dried CO_2 using a critical point-drier (CPD 030, Bal-TEC, Switzerland) for 30 mins. The cells were fixed on a metal SEM stub sputter coated in gold using the SEM coating unit (E5100 Polaron, UK). The coated samples were examined using SEM (JOEL 6400, Japan).

For TEM, the cells were seeded in 6-well plates at 5×10^5cells/well in 2 mL of complete growth medium, incubated for 24 hrs and treated with the IC_{50} of DOX (0.5 µg/mL) and DOX-NPs (with corresponding DOX concentration) for 48 hrs. Control cells were treated with complete growth medium only. After 48 hrs of incubation, the cells were rinsed with PBS and harvested. Subsequently, the cells were fixed with 4% glutaraldehyde for 24 hrs at 4°C and post-fixed with 1% osmium tetroxide at 4ºC for 2 hrs. Subsequent to each fixing, the cells were rinsed three times with 0.1 M sodium coccadylate buffer. Then, the cells were dehydrated with increasing concentrations of acetone (35%, 50%, 75%, 95%, and 100%). The cells were infiltrated with resin and embedded with 100% resin in beam capsule and then left to polymerize at 60ºC for 48 hrs. Thereafter, the selected area was cut into ultrathin sections using an ultra-microtome, placed onto copper grids, and stained with uranyl acetate and citrate. The stained samples were viewed using HRTEM (HRTEM: H-7100 Hitachi, Tokyo, Japan).

Statistical analysis

Statistical analysis was conducted using triplicate samples. The results are expressed as mean ± standard deviation and plotted in columnar graphs using the Origin 8.5 software (Origin Lab, MA, USA).

Results

Morphology and surface charge of $CaCO_3$_NPs and DOX-NPs

The morphology of the NPs before and after drug-loading displayed a homogeneous spherical shape, with a distributed size of 35.5 nm, under TEM (Figure 2). The image shows a porous characteristic in support of the synthesized NPs. FESEM before and after drug loading into the NPs depicted spherical shapes with an average diameter of 29.7±5 nm is shown in in Figure 3.

The zeta potential analysis shows the surface potential of −19.1±3.9 mV and avergae diameter of 167.2 nm of the NPs, respectively, at an average temperature of 24.0°C with a polydispersity index of 0.237 and 100% intensity as revealed in Figure 4. The zeta potential of – 17.8±4.6 mV of the loaded DOX-NPs is shown in Figure 4.

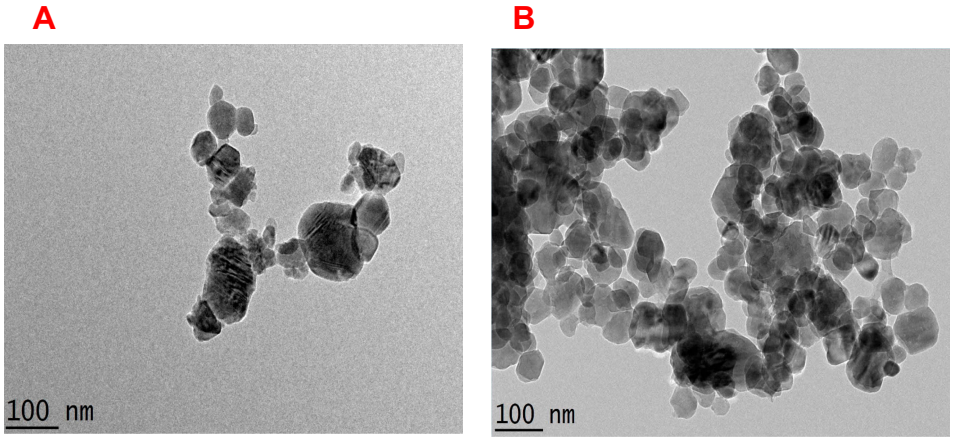

Figure 2 HRTEM morphology of NPs (**A**) before and (**B**) after drug loading on NPs.
Abbreviations: HRTEM, high-resolution transmission electron microscopy; NPs, nanoparticles.

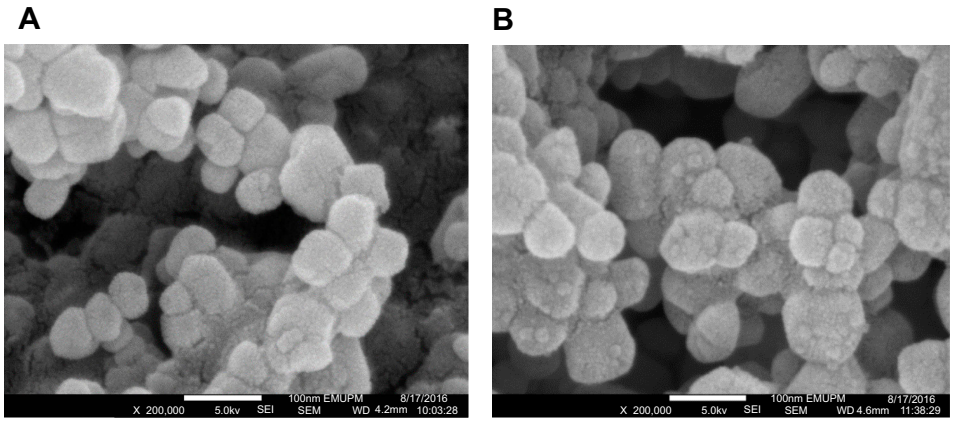

Figure 3 Field-emission scanning electron microscopy morphologies of nanoparticles (**A**) before and (**B**) after drug loading.

FT-IR analysis

The FT-IR spectra of NPs, DOX-NPs, and DOX are presented in Figure 5 at 1478, 1082, 860, and 712 cm^{-1}, respectively. The FT-IR spectra of DOX shows the presence of hydroxide (OH^-) and amino ($-NH_2$) functional groups. The absorption peak at 2931 cm^{-1} was attributed to the $-NH_2$ cluster of DOX, which overlapped with the broad band of OH^- as depicted in the structure of DOX. The presence of the distinctive peaks of DOX shows efficient loading of the drug into the NPs, as indicated in Figure 5.

XRD analysis

The XRD patterns of the $CaCO_3$-NPs, DOX, and DOX-NPs are shown in Figure 5. The XRD pattern of NPs was similar to the aragonite reference spectra in the Inorganic Crystal Database (ICSD) file no. 98-010-9084. In the same regard, the XRD pattern of DOX-NPs was comparable to that of the NPs. This indicates that the unique crystal nature of aragonite was not altered by drug loading.

Drug loading

DOX was loaded in NPs at different ratios. As revealed in Table 1, with increasing loading concentrations of DOX (1, 2, and 3 mg), higher loading contents were observed (6.25%, 12.9%, and 19.3%, respectively) while the loading efficiencies of the three formulations increased from 93.8% to 97%.

In vitro DOX release profile

As presented in Figure 6, the in vitro drug discharge profile of DOX from DOX-NPs (drug-loaded delivery-carrier in the first stage) simulated physiological conditions with excellent pH sensitivity (<36% pH 7.4). An extremely small amount of DOX was released in PBS at 70% gradually and sustainably within 72 hrs. More importantly, when DOX was exposed to an

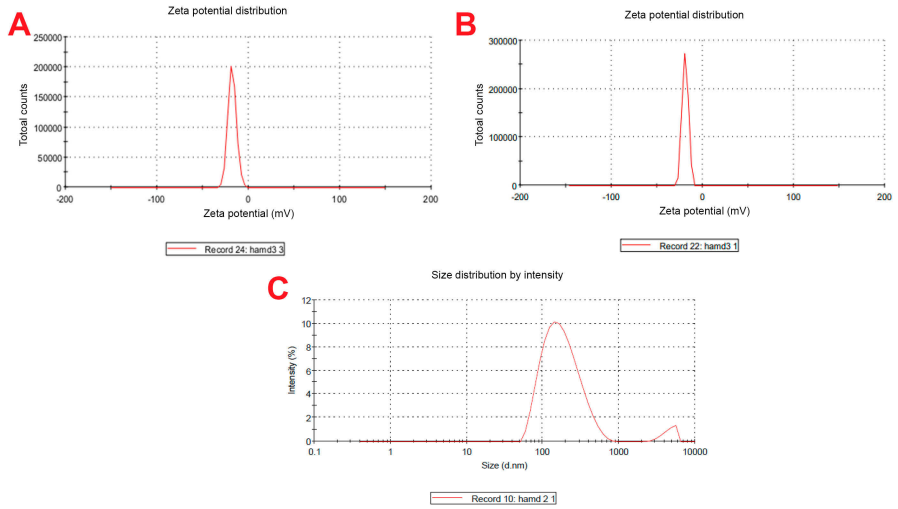

Figure 4 Zeta potential representations (**A**) showed the distribution of nanoparticles (NPs) derived from cockleshells, (**B**) doxorubicin NPs, and (**C**) zeta size representations.

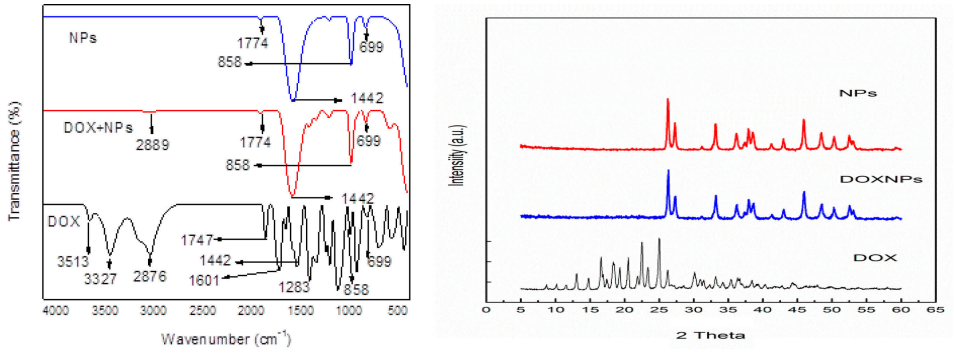

Figure 5 FT-IR and XRD patterns of NPs, DOX-NPs, and DOX.
Abbreviations: DOX, doxorubicin; NPs, nanoparticles; FT-IR, *Fourier-transform infrared spectroscopy*; XRD, x-*ray powder diffraction*.

Table 1 Drug loading concentrations, drug content, and encapsulation efficiency of doxorubicin nanoparticles (DOX-NPs)

Sample	Weight of nanoparticles (mg)	Weight of drug (DOX) (mg)	Loading content (%)	Encapsulation efficiency (%)
DOX-NP (1)	15	1	6.25	93.8
DOX-NP (2)	15	2	12.9	97.0
DOX-NP (3)	15	3	19.3	96.7

acidic environment at pH 4.8, sustainable release. Approximately 73% of the DOX was released speedily within 1 hr, and within a long period of 72 hrs, almost 74% of the total DOX was released at pH 4.8. In basic pH, 32% of DOX was released from $CaCO_3$-NPs within 2.5 hrs, and with increasing time, approximately 70% of DOX was released gradually within 4 hrs.

Morphological examinations

Inverted light microscopic images of MCF-7 cells were treated for 48 hrs with DOX and DOX-NPs. (A) Control cells (100X). (B) Cells treated with free NPs (100X). (C) Cells treated with free DOX (100X). (D) Cells treated with Dox-NPs (100X). Red arrows depict Cell shrinkage and detachment; yellow arrows depict DOX-NP Coacervates in Figure 7.

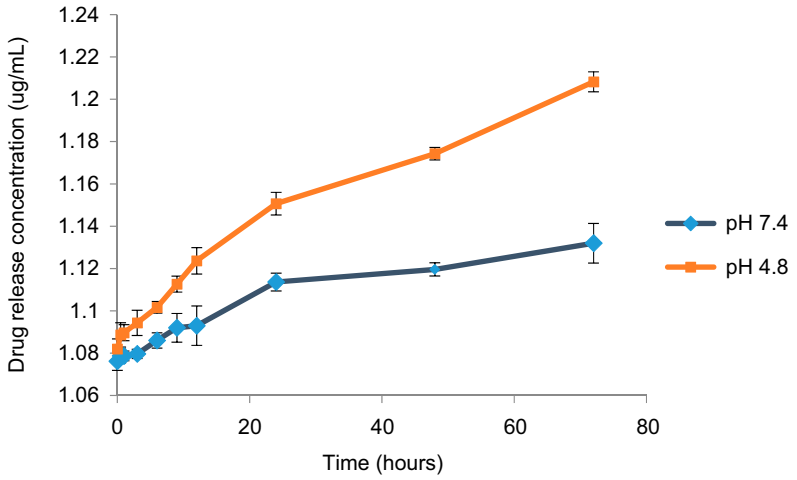

Figure 6 The in vitro drug release profile of DOX from doxorubicin nanoparticles (DOX-NPs) cell culture.

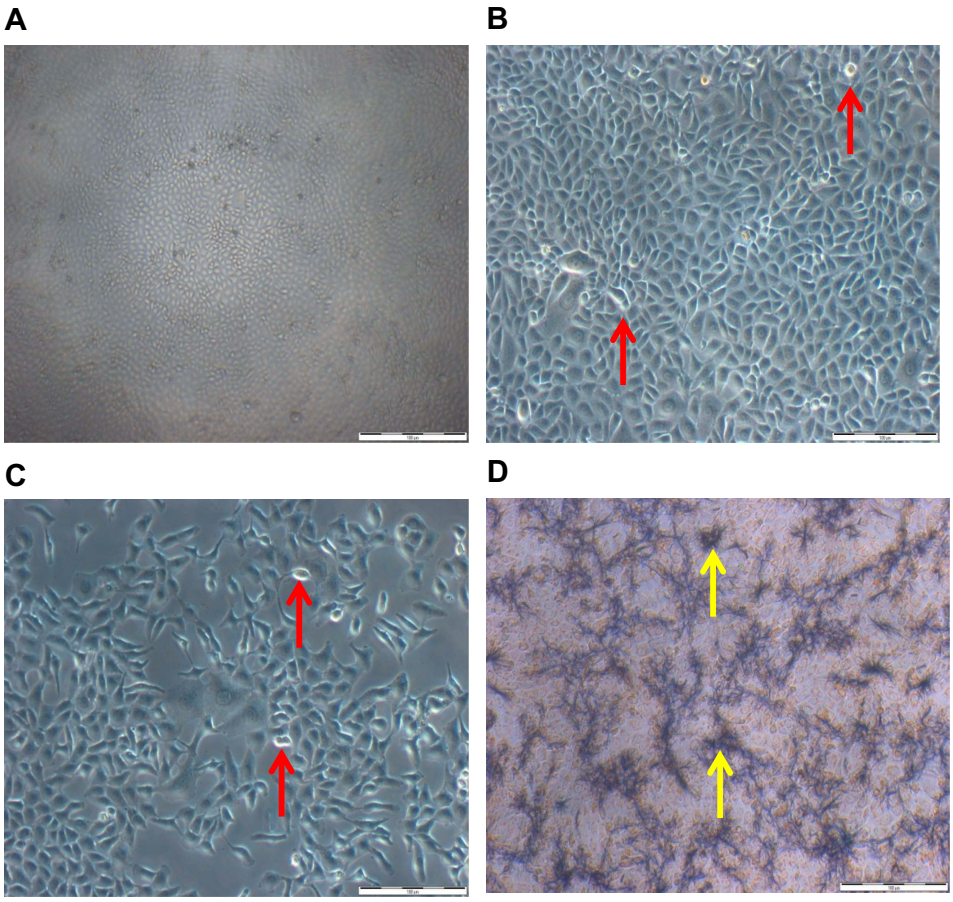

Figure 7 Morphology of MCF-7 cells treated for 48 hrs with DOX as well as doxorubicin nanoparticles (DOX-NPs). (**A**) Control cells (untreated). (**B**) Cells treated with free NPs. (**C**) Cells treated with DOX. (**D**) Cells treated with DOX-NPs. Red indicators portray cell shrinkage with detachment; yellow arrows portray DOX-NPs coacervates (scale bar: 100 μm).

MTT cytotoxicity assay for DOX and DOX-NPs

The cytotoxicity of DOX and DOX-encapsulated $CaCO_3$-NPs was investigated using MCF-7 cells via the MTT assay. MCF-7 cells were treated with different concentrations of DOX and DOX-NPs and incubated for 24, 48, and 72 hrs. The cell inhibition rate was dependent on the drug concentration and incubation period, as shown in Figure 8. MCF-7 cells were more susceptible to DOX than they were to DOX-NPs for 24 hrs and 48 hrs, while at 72 hrs, they were more sensitive to DOX-NPs than they were to free DOX.

Biocompatibility assay for cockle shell-aragonite $CaCO_3$ nanocrystals

The effect of cockle-shells derived $CaCO_3$ nanocrystals on MCF-7 cells was evaluated to verify the toxicity of the carrier for compatibility studies in the biological scheme (Figure 9). The MTT assay is based on the principle where mitochondrial oxidoreductase (NADP pH-dependent) enzymes convert the water-soluble yellow MTT tetrazolium dye into the insoluble purple formazan via cleavage of the tetrazolium ring. The formazan product is resistant to cell membranes with loss of integrity and consequently only accumulates inside healthy cells.

The analyzed results showed good biocompatibility of cockle shell $CaCO_3$ NPs and indicated zero apparent toxicity toward MCF-7 cells with greater than 92% cell viability, even at high concentrations of 800−1000 µg/mL.

Acridine orange and propidium iodide double staining is an excellent method of measuring the cell viability precisely as the dyes are permeable to both live and dead cells, enabling necrotic and apoptotic cell death to be distinguished. As demonstrated in Figure 10, healthy cells have round nuclei along with green staining, whereas apoptotic cells are stained red as a results cell blebbing and fragmented DNA is shown in orange.

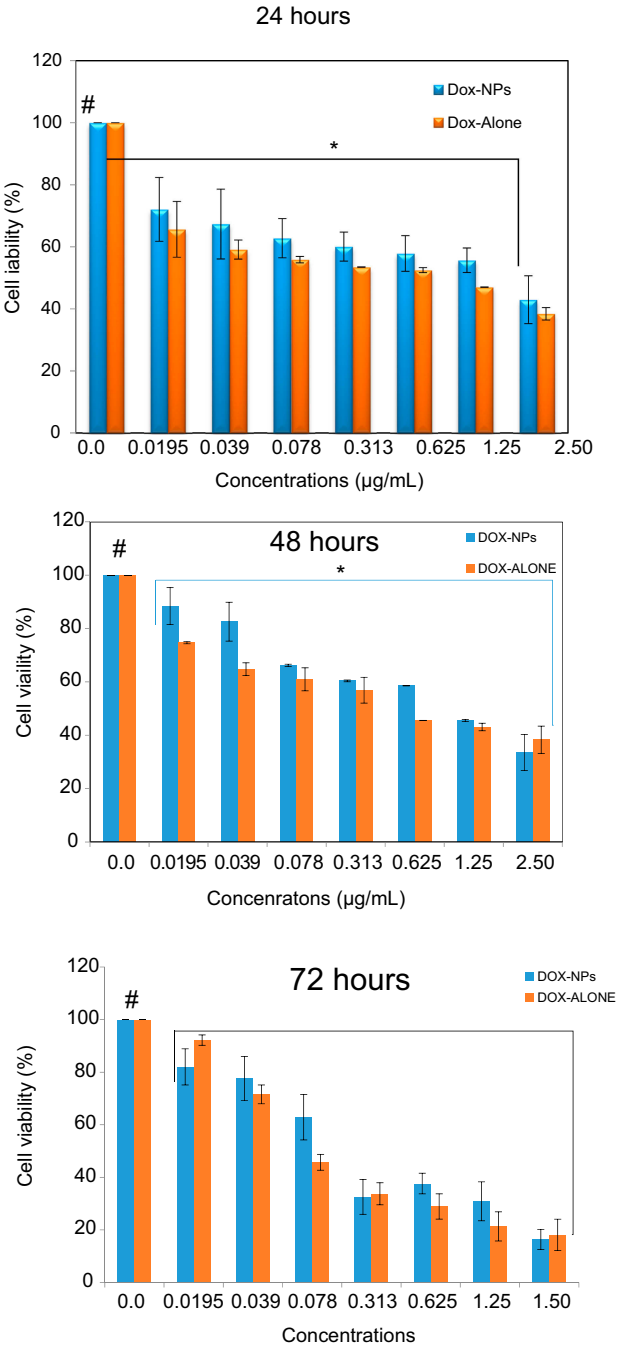

Figure 8 Cytotoxicity of DOX and doxorubicin nanoparticles (DOX-NPs) on MCF-7 cells with the IC_{50} for DOX-NPs and DOX at 24, 48, and 72 hrs, respectively. The means with asterisk (*) differed significantly ($p< 0.05$) with the normal untreated group (#).

Ultrastructural surface morphology of treated MCF-7 cells

SEM was performed to acquire detailed evidence of the ultrastructural surface alterations of MCF-7 cells upon treatment with DOX-NPs for 48 hrs at IC_{50}. The untreated cells revealed typical morphological structures of cancer cells, with numerous lamellipodia and microvilli on the surface (Figure 11A). Morphological alterations on the lamellipodia and microvilli were observed in the treatment groups (Figure 11B and C). Cells treated with DOX demonstrated a decrease in the quantity of microvilli along with observable deformation, even though the cells treated with DOX-NPs demonstrated a relatively polished surface with disappearing microvilli. Furthermore, in the treatment groups, separate apoptotic bodies, irregular

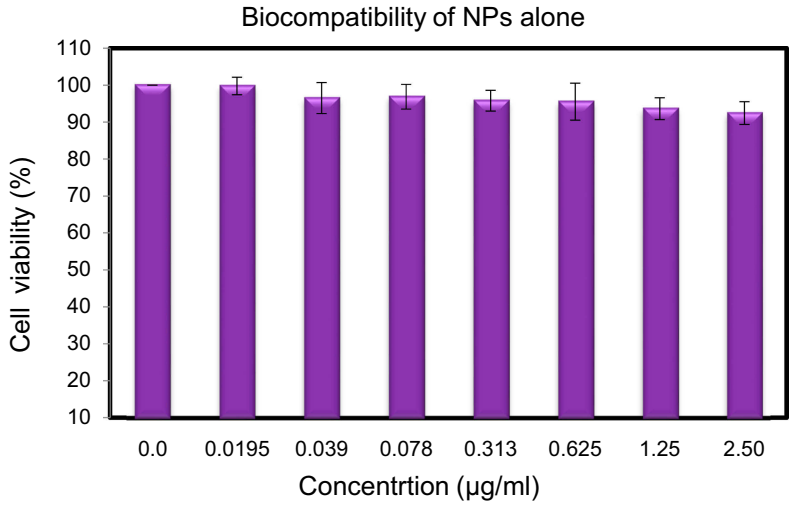

Figure 9 Biocompatibility of cockle shell–derived $CaCO_3$ nanoparticle (NP) on MCF-7 cells.

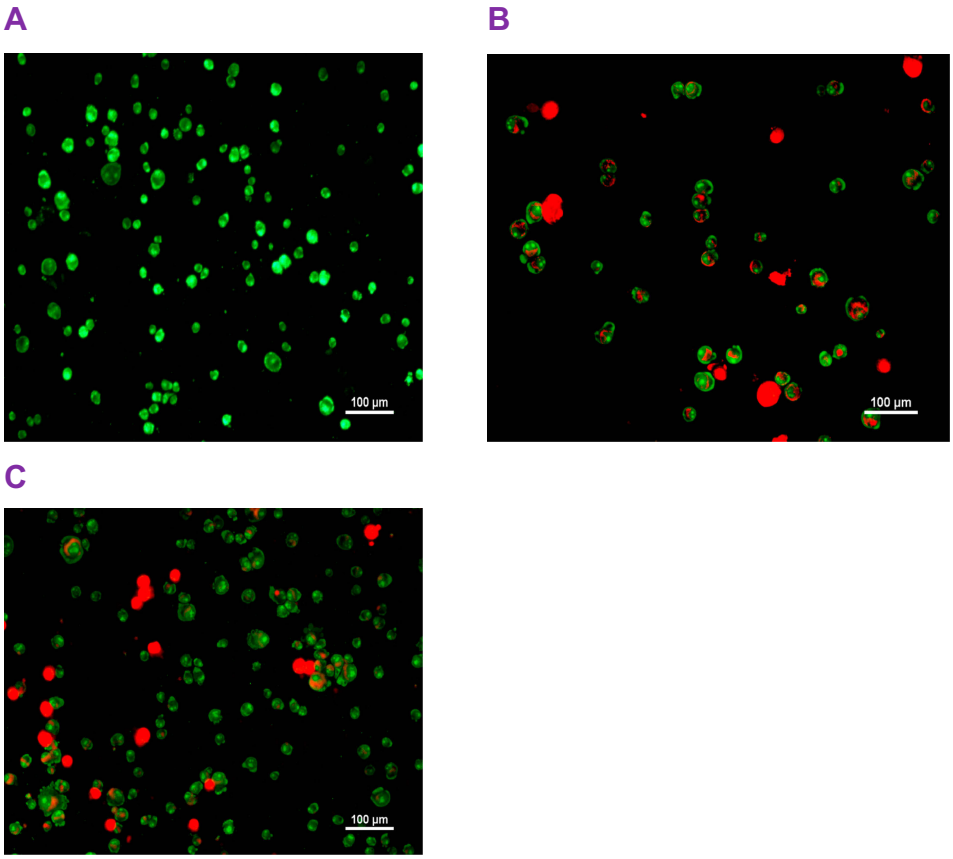

Figure 10 Fluorescent microscopy images of MCF-7 cells at 48 hrs stained by acridine orange and propidium iodide (AO/PI) (**A**) control MCF-7 cells (untreated), (**B**) treated with DOX, and (**C**) treated with doxorubicin nanoparticles (DOX-NPs). Scale bar: 100 µm.

plasma membranes, and cell shrinkage were evident. Cell shrinkage is a typical feature of early apoptosis and has been correlated with nuclear and cytoplasm manifestations of apoptosis (Figure 11).

Morphology of treated MCF-7 cells

The difference in cell morphology was examined to perceive the effect of DOX and DOX-NPs on MCF-7 cells via TEM. The ultrastructural features of MCF-7

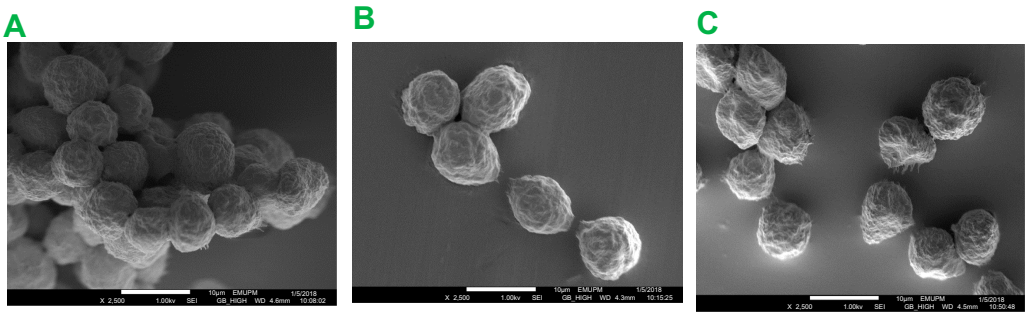

Figure 11 SEM micrographs of surface ultrastructural features. (**A**) Untreated MCF-7 cells. (**B**) MCF-7 cells treated with DOX exhibiting membrane blebbing, cell shrinkage with apoptotic body. (**C**) MCF-7 cells treated with $CaCO_3$NP-DOX exhibiting membrane blebbing, Cell shrinkage (25,000)×, bar 10 μm.
Abbreviations: DOX, doxorubicin; NPs, nanoparticles; SEM, scanning electron microscopy.

cells are exhibited in Figure 12 by electron micrographs. The micrographs of untreated cells and cockle shell NPs demonstrated well-distributed chromatin, clear nuclear membranes, and exposed cell organelles with complete integrity (Figure 12A). Notable alterations after treatment with DOX or DOX-NPs were

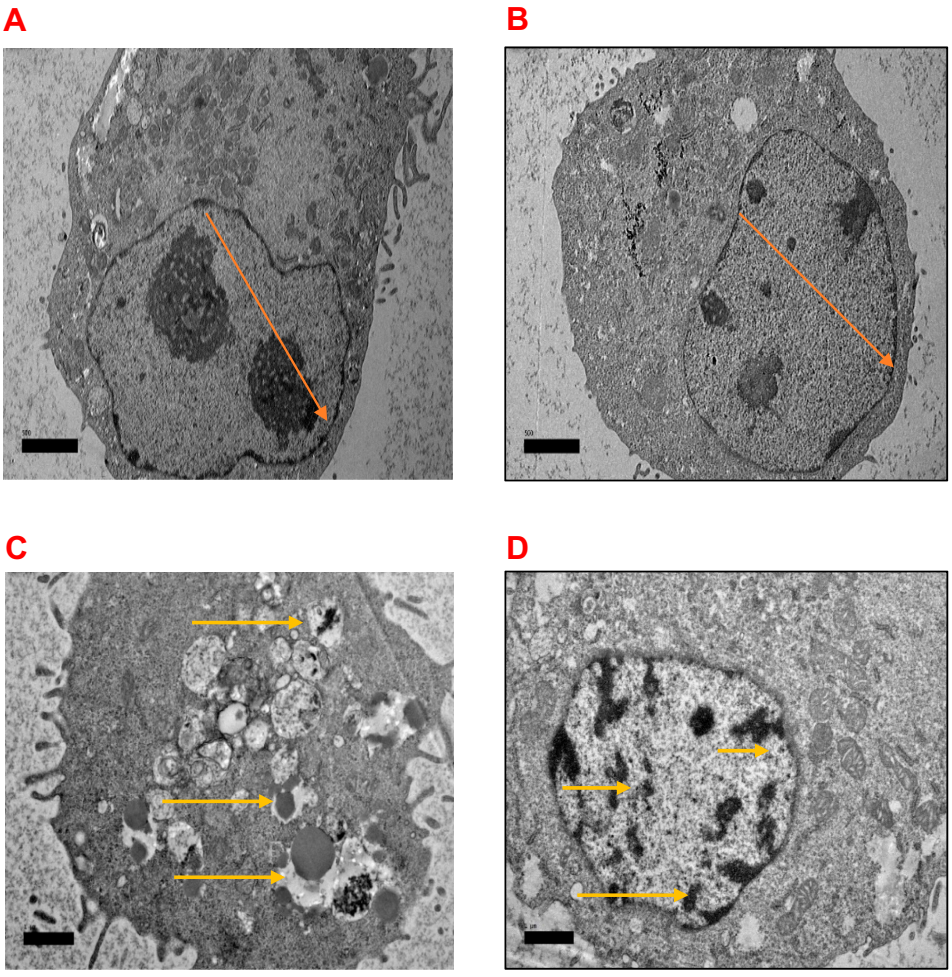

Figure 12 Electron micrographs of MCF-7 cells (**A**), control untreated cells and (**B**) treated with NPs exhibiting normal cellular method containing unabridged integrity of cells organelle, with rounded shaped cells containing nucleus and nucleolus chromatin (orange arrow) (**C**) Treated with DOX with switch nuclear collapse, progressing blebbing, apoptotic body formation (yellow arrow), and (**D**) treated with NP-DOX revealing chromatin condensation, bar 2 μm.
Abbreviations: DOX, doxorubicin; NPs, nanoparticles.

demonstrated with typical apoptotic phenomena (Figure 12C), with signs of early apoptosis such as chromatin condensation, cell shrinkage, and margination in both treatment groups. An enormous number of vesicles were present in the cytoplasm, and a small number of vacuoles containing DOX-NP coacervates were observed (Figure 12D). These designated DOX-NPs were able to internalize into cells. However, similar alterations were observed in Figure 12D.

Discussion

This study reports the development of doxorubicin-based aragonite NPs for the treatment of MCF7 luminal cell line. It highlights the cheap synthesis of cockle-shell derived $CaCO_3$-NPs under a mild and environmentally friendly condition and its effectiveness as a nano-carrier in cancer therapy. DOX is a potent chemotherapeutic agent used in the management of different cancer patients.[19] However, its off-target effect poses a potential threat to the patient due to induced cardiotoxicity. This has prompted the search for synthetic inorganic carriers with targeting ability to deliver DOX as a new strategy to ameliorate the off-target effects.[20]

As a remedy to the toxic effect of DOX, the potential of $CaCO_3$NPs loaded with DOX in breast cancer therapy is explored. The purity of the NPs was fortified by the use of banana pelt, instead of conventional bleaching agents as a means of cleansing the cockle shells of inherent dirt. This helped forestall reactivity and attendant impurity. Calcium carbonates are naturally abundant in the form of aragonite polymorph in seawater organisms.[21] The physicochemical properties of the synthesized $CaCO_3$-NPs are essential in drug delivery, which consequently improves therapeutic safety and efficacy.

In this study, the pleomorphic geometry of $CaCO_3$NPs after being loaded with DOX remained the same with more dispersed particles with a diameter of less than 40 nm. This geometry was similar to that reported in a previous study, where the toxicity and effectiveness of DOX were improved upon the use of nanomaterials of this nature.[22] The negative zeta potential and shape of the DOX-$CaCO_3$ NPs might have induced the increased loading content and targeting potential in the treatment of cancers cells.[5]

Based on the FT-IR spectra, the peaks were comparable to published reports[10,16,23,24] that utilized $CaCO_3$ nanocrystals for drug delivery and tissue engineering.

The spectral peaks observed on DOX-NPs indicate clear signature of both DOX and aragonite $CaCO_3$NPs as cited earlier,[17] with DOX showing signatory spectra at 3513 and 3327 cm. The presence of these spectra peaks strongly indicates the successful loading of DOX in the $CaCO_3$NPs. However, there were slight shifts in the spectra at 708 cm^{-1}, 1442 cm^{-1}, 1089 cm^{-1}, and 858 cm^{-1}, which might be due to the binding between the drug and the $CaCO_3$NPs. Moreover, the peaks of the functional groups were retained as seen in previous works whereby nano-encapsulation strategies were used to deliver DOX.[25,26] However, some new functional group peaks have emerged in these works.

The acquired diffraction spectra were similar to the conventional reference spectra of $CaCO_3$ (ICSD No 98-010-9084). In addition, the XRD spectra of $CaCO_3$ were similar to those that were synthesized using different methods.[4,27,28]

DOX was successfully loaded in the $CaCO_3$NPs, thus showing the high potential of these NPs as effective delivery vehicles for anticancer drugs. Minimal losses were demonstrated during the drug-loading process and these were attributed to the negative surface charge of electrostatic interactions. DOX-NPs were found to have more elevated loading content at 19.3% and were thus chosen for drug delivery.

Our drug release results agree with those in previous studies utilizing different NP droplets as delivery vehicles for DOX. In these studies, the peak DOX release was observed after 3 hrs with sustained release of DOX in a slow manner in the medium at physiological pH. This was similar to the previous reports,[17,28] indicating enhanced bioavailability.

Additionally, previous literature has reported that the higher cytotoxicity of drugs formulated into NPs could be ascribed to the combination of diverse but not exclusive mechanisms. The formulated particles were absorbed through the cell surface, resulting in increased drug concentration in the cell membrane, which in turn generates viability and a concentration gradient that aids in the influx of the drug into the cell.[29] DOX is delivered into the cell cytoplasm via the process of passive diffusion. On the other hand, $CaCO_3$-NPs are taken up by cells through endocytosis, which results in the increased cytotoxicity DOX-loaded NPs, allowing it to bypass ejection from cell by P-gp pumps.[18]

However, Kamba et al (2013) reported lower cell viability, following treatment of cells with 2 μg/mL DOX for two days; verifies the sustained release of DOX from the multilayer NPs. These differences in cytotoxicity are explained by many scholars as a result of the effects of DOX on cell viability.[30] Free DOX is mediated through a passive diffusion mechanism and thereby directly affects normal cells, whereas in the case of DOX-NPs, the DOX is released in a time-dependent manner from the $CaCO_3$ NPs before it exerts its effects on the cells.

The size, shape, and zeta potential of nano-carriers are likely to induce apoptosis as observed in similar inorganic NPs.[29] As an NPs drug delivery vehicle, $CaCO_3$ was demonstrated to be biocompatible and non-toxic. This finding is in line with previous reports,[12,18] where $CaCO_3$NPs showed good cytocompatibility with MG 63 cells. Therefore, the application of $CaCO_3$ in recent years has advanced beyond drug delivery. Significant research effort is being devoted to the development of effective cancer therapy in biomedical applications.[31]

Our treatments resulted in different morphological modifications, which are typical features of apoptosis.[32,33] These results provide proof that DOX-NPs can induce apoptosis in MCF-7 cells.

The characteristic features and ultrastructural alterations in MCF-7 cells were observed by SEM. Cell shrinkage is the most characteristic feature of early apoptosis.[34] Membrane blebbing is one of a sequence of typical morphological measures during apoptosis.[34] Apoptosis yields cell fragments called apoptotic bodies, the presence of which suggests that cells are in the late phase of apoptosis. Our treatments resulted in separate morphological modifications that are typical features of apoptosis.[35] The most important signs of early apoptosis are cell shrinkage, margination, and chromatin condensation, which were observed in both treatment groups.[34] Characteristic apoptotic phenomena, including membrane blebbing and apoptotic bodies, were also observed, showing that DOX-NPs were able to induce apoptosis in breast cancer cells.

The method used in this study employs a simple synthesis technique with a slight modification that avoided the involvement of stringent temperatures and monotonous gas frothing. Normally, high drug-loading ability is vital in achieving desirable drug efficacy for long-term drug carriers and this has been achieved. In addition, the $CaCO_3$NPs showed good biocompatibility with cells. Following DOX loading, DOX-NPs displayed pH-sensitive drug release properties. However, to the best of our knowledge, data on the use of banana pelts is on record for the treatment of cockle shells used in the synthesis of NPs.

Acknowledgments

The authors wish to acknowledge the support of the staffs of Microscopy laboratory unit, Institute of Bioscience and the Biochemistry unit, Universiti Putra Malaysia, for their assistance during the analysis. This research was funded by the Universiti Putra Grant (IPS/9578300) and the Fundamental Research Grant Scheme (FRGS/5540031)

Disclosure

The authors declare no conflicts of interest in this work.

References

1. Acar H, Srivastava S, Chung EJ, et al.Self-assembling peptide-based building blocks in medical applications. *Adv Drug Deliv Rev*. 2017;(110):65–79. doi:10.1016/j.addr.2016.08.006
2. Peppas NA, Hilt JZ, Khademhosseini A, Langer R. Hydrogels in biology and medicine: from molecular principles to bionanotechnology. *Adv Mater*. 2006;18:1345–1360. doi:10.1002/(ISSN)1521-4095
3. Mansor R. Proteomic and metabolomic studies on milk during bovine mastitis. 2012.
4. Saidykhan L, Bakar MZBA, Rukayadi Y, Kura AU, Latifah SY. Development of nanoantibiotic delivery system using cockle shell-derived aragonite nanoparticles for treatment of osteomyelitis. *Int J Nanomedicine*. 2016;11:661–673. doi:10.2147/IJN.S95885
5. Fu W, Hezmee M, Noor M, et al. In vitro evaluation of a novel pH sensitive drug delivery system based cockle shell-derived aragonite nanoparticles against osteosarcoma. *J Exp Nanosci*. 2017;12(1):166–187. doi:10.1080/17458080.2017.1287965
6. Bazak R, Houri M, El Achy S, Kamel S, Refaat T. Cancer active targeting by nanoparticles: a comprehensive review of literature. *J Cancer Res Clin Oncol*. 2015;141(5):37–54. doi:10.1007/s00432-014-1767-3
7. Yang J, Guo W, Wang L, et al. Notch signaling is important for epithelial-mesenchymal transition induced by low concentrations of doxorubicin in osteosarcoma cell lines. *Oncol Lett*. 2017;13(4):2260–2268. doi:10.3892/ol.2017.5708
8. Shafiu Kamba A, Zakaria ZAB. Osteoblasts growth behaviour on bio-based calcium carbonate aragonite nanocrystal. *Biomed Res Int*. 2014;2014:215097. doi:10.1155/2014/215097
9. Maliepaard M, Scheffer GL, Faneyte IF, et al. Subcellular localization and distribution of the breast resistance protein transporter in normal human tissues. *Cancer Res*. 2001;61(8):3458–3464.
10. Islam KN, Bakar MZBA, Ali ME, et al. A novel method for the synthesis of calcium carbonate (aragonite) nanoparticles from cockle shells. *Powder Technol*. 2013;235:70–75. doi:10.1016/j.powtec.2012.09.041
11. Shafiu Kamba A, Ismail M, Tengku Ibrahim TA, Zakaria ZAB. A pH-sensitive, biobased calcium carbonate aragonite nanocrystal as a novel anticancer delivery system. *Biomed Res Int*. 2013;2013:587451. doi:10.1155/2013/587451
12. Shafiu Kamba A, Ismail M, Tengku Ibrahim TA, Zakaria ZAB. Synthesis and characterisation of calcium carbonate aragonite nanocrystals from cockle shell powder (*Anadara granosa*). *J Nanomater*. 2013;2013.

13. Ali ME, Hashim U, Mustafa S, et al. Nanoparticle sensor for label free detection of swine DNA in mixed biological samples. *Nanotechnology*. 2011;22(19):195503. doi:10.1088/0957-4484/22/19/195503
14. Wei W, Hu G, Yu D, et al. Preparation of hierarchical hollow CaCO 3 particles and the application as. *J Am Chem Soc*. 2008;130:15808–15810. doi:10.1021/ja8039585
15. Paramasivam G, Kayambu N, Rabel AM, Sundramoorthy AK, Sundaramurthy A. Anisotropic noble metal nanoparticles: synthesis, surface functionalization and applications in biosensing, bioimaging, drug delivery and theranostics. *Acta Biomater*. 2017;49:45–65. doi:10.1016/j.actbio.2016.11.066
16. Hoque E, Shehryar M, Islam KN. Material Science & Engineering processing and characterization of cockle shell calcium carbonate ($CaCO_3$) bioceramic for potential application in bone tissue engineering. *J Mater Sci Eng*. 2013;2(4):2–6.
17. Danmaigoro A, Selvarajah GT, Noor MHM, Mahmud R, Zakaria MZAB. Development of cockleshell (Anadara granosa) derived $CaCO_3$ nanoparticle for doxorubicin delivery. *J Comput Theor Nanosci*. 2017;14(10):5074–5086. doi:10.1166/jctn.2017.6920
18. Hammadi NI, Abba Y, Hezmee MNM, et al. Formulation of a sustained release docetaxel loaded cockle shell-derived calcium carbonate nanoparticles against breast cancer. *Pharm Res*. 2017;34 (6):1193–1203. doi:10.1007/s11095-017-2135-1
19. Milic V, Dragojevic V. Doxorubicin-induced oxidative injury of cardiomyocytes - do we have right strategies for prevention?. *Cardiotoxicity Oncol Treat*. 2012;89–130.
20. Qin W, Huang G, Chen Z, Zhang Y. Nanomaterials in targeting cancer stem cells for cancer therapy. *Front Pharmacol*. 2017;8:1. doi:10.3389/fphar.2017.00001
21. Jimoh OA, Ariffin KS, Bin HH, Temitope AE. Synthesis of precipitated calcium carbonate: a review. *Carbonates Evaporites*. 2017;1–16.
22. Dizaj SM, Barzegar-Jalali M, Zarrintan MH, Adibkia K, Lotfipour F. Calcium carbonate nanoparticles as cancer drug delivery system. *Expert Opin Drug Deliv*. 2015;12(10):1649–1660. doi:10.1517/17425247.2015.1049530
23. Guo F, Li Y, Xu H-X, Zhao G-Q, He X-J. Size-controllable synthesis of calcium carbonate nanoparticles using aqueous foam films as templates. *Mater Lett*. 2007;61(27):4937–4939. doi:10.1016/j.matlet.2007.03.075
24. Shirsath SR, Bhanvase BA, Sonawane SH, Gogate PR, Pandit AB. A novel approach for continuous synthesis of calcium carbonate using sequential operation of two sonochemical reactors. *Ultrason Sonochem*. 2017;35:124–133. doi:10.1016/j.ultsonch.2016.09.009
25. Fernandez-Fernandez A, Manchanda R, McGoron AJ. Theranostic applications of nanomaterials in cancer: drug delivery, image-guided therapy, and multifunctional platforms. *Appl Biochem Biotechnol*. 2011;628–1651.
26. Press D. Inorganic nanolayers : structure, preparation, and biomedical applications. 2015;5609–5633.
27. Jaji AZ, Bin Z, Bakar A, Mahmud R. Synthesis, characterization, and cytocompatibility of potential cockle shell aragonite nanocrystals for osteoporosis therapy and hormonal delivery. 2017;23–33. doi:10.1142/S0218810417500046
28. Khiri MZA, Matori KA, Zainuddin N, et al. The usability of ark clam shell (*Anadara granosa*) as calcium precursor to produce hydroxyapatite nanoparticle via wet chemical precipitate method in various sintering temperature. *Springerplus*. 2016;5(1):1206. doi:10.1186/s40064-016-2824-y
29. Berardi A, Bisharat L, Cespi M, et al. Controlled release properties of zein powder filled into hard gelatin capsules. *Powder Technol*. 2017;320(320):703–713. doi:10.1016/j.powtec.2017.07.093
30. Wei L, Surma M, Gough G, et al. Dissecting the mechanisms of doxorubicin and oxidative stress-induced cytotoxicity: the involvement of actin cytoskeleton and ROCK1. *PLoS One*. 2015;10(7).
31. Peng H, Li K, Wang T, et al. Preparation of hierarchical mesoporous CaCO3by a facile binary solvent approach as anticancer drug carrier for etoposide. *Nanoscale Res Lett*. 2013;8(1):321. doi:10.1186/1556-276X-8-321
32. Dewangan J, Kaushik S, Rath SK, Balapure AK. Centchroman regulates breast cancer angiogenesis via inhibition of HIF-1α/VEGFR2 signalling axis. *Life Sci*. 2018;193:9–19. doi:10.1016/j.lfs.2017.11.045
33. Khazaei S, Esa NM, Ramachandran V, et al. In vitro antiproliferative and apoptosis inducing effect of *Allium atroviolaceum* bulb extract on breast, cervical, and liver cancer cells. *Front Pharmacol*. 2017;8:5. doi:10.3389/fphar.2017.00005
34. Brauchle E, Thude S, Brucker SY, Schenke-Layland K. Cell death stages in single apoptotic and necrotic cells monitored by Raman microspectroscopy. *Sci Rep*. 2014;14(10):5074–5086.
35. Sasikala ARK, Unnithan AR, Thomas RG, et al. Correction to: multifaceted implantable anticancer device for potential postsurgical breast cancer treatment: a single platform for synergistic inhibition of local regional breast cancer recurrence, surveillance, and healthy breast reconstruction. *Adv Funct Mater*. 2018. doi:10.1002/adfm.201704793